





Original Research

MAP7 Mediates Tumorigenicity in Human Ovarian Cancer Cells: A Prospective Laboratory Evaluation of Malignant Tissues

Xiao Shi¹, Zhendong Qin¹, Guangming Cao^{1,*}, Xiaoli Ru^{2,*}

¹Center for Reproductive Medicine, Beijing Chaoyang Hospital, Capital Medical University, 100020 Beijing, China

²Department of Obstetrics and Gynecology, Beijing Chaoyang Hospital, Capital Medical University, 100020 Beijing, China

*Correspondence: caoguangming_2009@126.com (Guangming Cao); xiaoliru2012@163.com (Xiaoli Ru)

Academic Editors: Kenny Chitcholtan and Michael H. Dahan

Submitted: 4 February 2025 Revised: 27 June 2025 Accepted: 18 July 2025 Published: 31 July 2025

Abstract

Background: Ovarian cancer (OC) is among the most common types of cancer affecting the female reproductive system, second only to cervical cancer in incidence. Recent studies have identified Microtubule associated protein 7 (MAP7) as a key factor influencing the malignant characteristics of various tumor cell types. However, the expression levels and functional roles of MAP7 in OC remain insufficiently characterized. This study aims to explore the expression profile of MAP7 and its functional implications in OC, with the goal of clarifying its potential contribution to tumor development and the underlying molecular mechanism. **Methods:** The MAP7 expression in OC was assessed using data from The Cancer Genome Atlas (TCGA), Genotype-Tissue Expression (GTEx), and The Human Protein Atlas (HPA) databases. A tissue microarray assay (TMA) was constructed to evaluate protein expression. Study gene function was investigated through MAP7 silencing and overexpression experiments in A2780 and SKOV3 OC cell lines. Cell proliferation and invasion/migration assays were conducted to assess cellular proliferation and mobility, respectively. Western blotting was performed to analyze related signaling pathways, while tumor formation in nude mice assessed *in vivo* tumorigenicity. **Results:** Data from TCGA and GTEx databases showed MAP7 overexpression in OC tissues, consistent with the findings from our local dataset. MAP7 mediated cell invasion, migration, and promoted cell proliferation in OC cells via the Protein Kinase B/mammalian Target of Rapamycin (Akt/mTOR) signaling pathway ($p < 0.05$). MAP7 knockdown significantly inhibited the tumorigenicity of OC cells in nude mice ($p < 0.05$). **Conclusions:** Our results highlight the role of MAP7 in the progression of OC. Given its involvement in Akt/mTOR signaling and tumorigenicity in preclinical models, MAP7 represents a novel potential therapeutic target for OC that warrants further investigation.

Keywords: ovarian cancer; MAP7; Akt/mTOR signaling pathway; biofunctions; tumorigenicity

1. Introduction

Ovarian cancer is among the most prevalent malignant tumors affecting the female reproductive system. Its subtle onset and absence of noticeable early symptoms [1] make early diagnosis especially difficult, leading to many patients being diagnosed at advanced stages, contributing to a 5-year survival rate of less than 30%. It has the highest mortality rate among gynecological cancers [2,3]. Traditional treatment for ovarian cancer typically involves surgical procedures, such as radical resection or debulking, followed by platinum-based chemotherapy. However, many patients develop resistance to these treatments, and the likelihood of recurrence is high, which further lowers survival rates [4,5]. Therefore, there is an urgent need to investigate new strategies for the early diagnosis of ovarian cancer. In recent years, extensive research has focused on understanding the molecular mechanisms that drive the progression of ovarian cancer, which could lead to the development of innovative targeted therapies and improve 5-year survival rates.

Microtubule-associated proteins (MAPs) play a crucial role in binding to microtubules, which helps maintain their stability and supports various cellular functions

such as cell polarization, division, and differentiation [6]. Among these proteins, Microtubule associated protein 7 (MAP7) stands out due to its high expression in epithelial cells and moderate levels in neuronal cells [7,8]. Research has shown that MAP7 is vital for cell proliferation and differentiation; it promotes microtubule growth, facilitates organelle transport by recruiting kinesin-1 to microtubules, and regulates microtubule polymerization and centrosome separation during cell division [9–11]. Furthermore, MAP7's interaction with kinesin motors is key to controlling organelle trafficking, which may influence the remodeling of the tumor microenvironment. Despite these insights, the specific role of MAP7 in ovarian cancer has not been thoroughly explored. Considering the aggressive nature and high recurrence rates of ovarian malignancies, understanding the molecular mechanisms involving MAP7 could lead to the development of new therapeutic strategies. This study aims to address this knowledge gap, highlighting MAP7 as a potential diagnostic and therapeutic target in ovarian cancer.



In this study, The Cancer Genome Atlas (TCGA) database and our local ovarian cancer sample analysis showed that MAP7 is upregulated in ovarian cancer. Functional assays showed that MAP7 promotes ovarian cancer cell invasion, migration, and proliferation, while MAP7 knockdown using lentivirus-mediated short hairpin RNA (Lv-shRNA) reduced tumorigenesis in nude mice. Thus, our experiments showed MAP7 is involved in the tumorigenicity of human ovarian cancer.

2. Materials and Methods

2.1 TCGA and GTEx Gene Expression Data

Gene expression data from TCGA and Genotype-Tissue Expression (GTEx) were analyzed through gene expression profiling and interactive analyses (<http://gepia.cancer-pku.cn/index.html>). Immunohistochemical data from TCGA were sourced from the Human Protein Atlas (<https://www.proteinatlas.org/humanproteome/tissue>).

2.2 Tissue-microarray (TMA)

This analysis involved a group of 45 patients diagnosed with ovarian cancer, all of whom received their diagnosis and treatment at Beijing Chaoyang Hospital, affiliated with Capital Medical University, between January 2016 and September 2020. To identify the primary tumor location, a histological examination was conducted using hematoxylin and eosin (HE)-stained slides. For each sample, a single 1-mm diameter tissue core was extracted and manually embedded into a recipient paraffin block using a manual tissue arrayer.

TMA sections, each 5 μ m thick, were dewaxed in xylene for 15 minutes. They were then rehydrated through a series of ethanol concentrations and rinsed with phosphate-buffered saline. To inhibit endogenous peroxidase activity, the sections were treated with a 3% hydrogen peroxide solution in methanol for 30 minutes. Antigen retrieval was performed using a microwave method with a citric acid buffer at pH 6.0. After this, the sections were incubated at room temperature for one hour in a 5% bovine serum albumin (BSA) solution (Cat# A8010, Solarbio, Beijing, China). The TMA sections were then incubated overnight at 4 °C with a rabbit anti-MAP7 antibody (1:100, Cat# ab240695, Abcam, Cambridge, UK), diluted in 5% BSA solution. Following this, they were treated with a horseradish peroxidase (HRP)-conjugated goat anti-rabbit secondary antibody (1:100, Cat# PV6001, ZSBG-BIO, Beijing, China), for one hour at room temperature. The sections were then exposed to 500 μ L of 3,3'-diaminobenzidine (DAB) (Cat# PV6001, ZSBG-BIO, Beijing, China) for one minute followed by staining with hematoxylin for 30 seconds and dehydration. The sections were then mounted following standard protocols and staining scores were assessed using Image Pro Plus (version 6.0; Media Cybernetics, Rockville, MD, USA).

$$\text{H-SCORE} = \sum (\text{PI} \times \text{I}) = (\text{percentage of cells of weak intensity} \times 1) + (\text{percentage of cells of moderate intensity} \times 2) + (\text{percentage of cells of strong intensity} \times 3).$$

2.3 Cell Lines and Culture Conditions

Human ovarian cancer cell lines SKOV3 (HTB77) was purchased from the American Type Culture Collection (ATCC, Manassas, VA, USA). Human ovarian cancer cell lines A2780 (SCSP-5477) was purchased from the Cell Bank of the Chinese Academy of Sciences (Shanghai, China). The two cells were cultured in RPMI-1640 medium (Cat# 11875093, Gibco, Waltham, MA, USA) supplemented with 10% fetal bovine serum (FBS; Cat# 10270106, Gibco, Waltham, MA, USA) and 1% penicillin/streptomycin (Cat# 15140122, Thermo Fisher Scientific, Waltham, MA, USA), and maintained at 37 °C in a 5% CO₂ humidified incubator. All the cell lines are obtained from the Chinese Academy of Sciences at 2018. We tested for mycoplasma contamination and verified cells by short tandem repeat (STR) test; morphology was confirmed by pathologist before the experiments. Before the experiment began, we excluded mycoplasma contamination by RT-PCR.

2.4 Production of Plasmid and Lentiviral Particles

The *in vitro* cell experiment used siRNA transfection and overexpression plasmids to infect the expression of MAP7. The following siRNA sequences were used: si-MAP7, 5'-CAGCTACAAAGTGCAAGATAAGA-3', si-NC: 5'-TTCTCCGAACGTGTCACGTTT-3'. Full-length fragment of MAP7 was synthesized and inserted into the pcDNA3.1 plasmid. Transfection was performed using lipo2000, and cells were collected for transfection efficiency detection 48 hours after transfection.

The cells used in the tumorigenicity assay in nude mice were established as stable transfected cell lines through lentiviral transfection. The specific short hairpin RNAs (shRNAs) targeting the MAP7 gene and scrambled shRNA (negative control, NC) were cloned into the GV248 plasmid. The following shRNA sequences were used: sh-MAP7, 5'-ACCATGAATCTTTCGAAATAT-3'. The MAP7 cDNA was ligated into a lentiviral vector, the GV492 plasmid, to amplify the MAP7 gene. The MAP7 cDNA was ligated into a lentiviral vector, the GV492 plasmid, to amplify the MAP7 gene.

2.5 RNA Extraction, Reverse Transcription, and Real-time PCR

Total RNA was extracted from either cells or tissues using TRIzol (Cat# 15596026, Thermo Fisher Scientific, Waltham, MA, USA), following the manufacturer's instructions. For reverse transcription, 1 μ g of RNA was used with a PrimeScript RT reagent kit that contains a gDNA eraser (Takara Bio, RR047A, Kusatsu, Japan). Quantitative reverse transcription polymerase chain reaction (qRT-

PCR) was performed using a Roche Light Cycler 480 II detection system (Roche, Basel, Switzerland). The detection of cDNA was carried out according to the instructions supplied with the SYBR® Premix Ex Taq™ kit (Cat# RR420A, Takara Bio, Shiga, Japan). Each sample was analyzed in duplicate, starting with an initial denaturation step at 95 °C for 30 seconds, followed by 40 cycles of 95 °C for 5 seconds and 60 °C for 31 seconds. The relative expression of MAP7 was normalized to the glyceraldehyde-3-phosphate dehydrogenase (GAPDH) value. The PCR primers used for real-time PCR were: *MAP7*, TCATCATGCCCTACAAAGCTG (forward) and TGCCAGATGTGAGGAAGAGTA (reverse); *GAPDH*, AAGGTCATCCTGAGCTGAAC (forward) and ACGCCTGCTTCACACCTTCT (reverse). The relative mRNA expression levels were calculated using the $2^{-\Delta CT}$ method.

2.6 Western Blot

Protein was extracted from both cells and tissues utilizing a lysis buffer designed for radioimmunoprecipitation assays (Solarbio, R0010, Beijing, China), which included inhibitors for protease and phosphatase (Solarbio, IKM1020, Beijing, China). A total of 30 µg of proteins extracted from cells and tissues were loaded onto 10% acrylamide gels for sodium dodecyl sulfate-polyacrylamide gel electrophoresis (SDS-PAGE) analysis. The proteins separated through electrophoresis were transferred to nitrocellulose membranes (Millipore, St Quentin-Yvelines, France) and incubated overnight with specific antibodies. Following this, a second incubation with HRP-conjugated antibodies (ZSGB-BIO, PV6001, Beijing, China) was performed. The resulting films were digitized using a calibrated BioRad GS 800 densitometer, and the signals were quantified with Image J software (National Institutes of Health, Bethesda, MD, USA). The antibodies used in this study included p-Akt (1:100, ab81283, Abcam, Cambridge, UK), Akt (1:100, ab8805, Abcam, Cambridge, UK), p-mTOR (1:100, ab109268, Abcam, Cambridge, UK), mTOR (1:100, ab32028, Abcam, Cambridge, UK), MAP7 (1:100, ab240695, Abcam, Cambridge, UK), p62 (1:100, ab109012, Abcam, Cambridge, UK), LC3B (1:100, ab192890, Abcam, Cambridge, UK), Beclin1 (1:100, ab302669, Abcam, Cambridge, UK), and GAPDH (1:1000, ab8245, Abcam, Cambridge, UK), all obtained from Abcam.

2.7 Transwell Insert Invasion and Migration Assay

The invasion assay was conducted using 24-well inserts with membranes (Corning Costar, 3422, Kennebunk, ME, USA), following established protocols. A2780 and SKOV3 cell lines were trypsinized and then plated into transwell inserts that had been pre-coated with 200 µg/mL of matrigel (BD Biosciences, 356234, Franklin Lakes, NJ, USA) at a density of 5×10^4 cells per insert. The upper chambers were filled with RPMI 1640 medium containing

0.1% FBS, while the lower chambers contained RPMI 1640 medium supplemented with 10% FBS. After 30 hours, the cells were fixed and stained with crystal violet. The cells that adhered to the upper side of the membrane were carefully removed, and the number of stained cells on the lower side of the membrane was counted using a light microscope.

2.8 Cell Proliferation Assay With Counting Kit-8 (CCK-8)

Cells were seeded at a density of 3×10^3 cells per well across six wells in 96-well plates, with each condition replicated six times. The CCK-8 reagent (Solarbio, CA1210, Beijing, China) was introduced to four separate 96-well plates following incubation periods of 0, 4, 24, 48, or 72 hours. Subsequently, after a 2-hour incubation with the CCK-8 reagent, absorbance was measured at a wavelength of 450 nm utilizing an enzyme-linked immunosorbent assay (ELISA) plate reader. This assay was conducted in triplicate to ensure reproducibility.

2.9 HE and IHC Staining

Tumor tissues were harvested and fixed in paraformaldehyde for 24 hours. The paraffin-embedded specimens were cut into 4 µm sections before staining with HE and immunohistochemistry (IHC). A MAP7 polyclonal antibody (Abcam, ab240695, Cambridge, UK), diluted 1:100 in 5% BSA, was then applied. An HRP-conjugated goat anti-rat IgG (Abcam, ab6721, Cambridge, UK) was used as the secondary antibody. The staining was then performed using a DAB-containing solution (ZSGB-BIO, ZLI9018, Beijing, China).

2.10 Xenografts

All procedures performed in animal studies were approved by the Animal Research Ethics Committee of Capital Medical University (AEEI-2022-006). A2780 human ovarian cancer cells (cultured in RPMI-1640 medium supplemented with 10% FBS and 1% penicillin/streptomycin at 37 °C in 5% CO₂) were trypsinized using 0.25% trypsin-EDTA (Gibco, 25200056, Waltham, MA, USA) for 3 min at 37 °C, pelleted by centrifugation at $300 \times g$ for 5 min, washed twice with PBS, and resuspended in ice-cold PBS at a density of 3×10^6 cells/100 µL. Twenty-four female BALB/c nude mice (4-week-old, 12–16 g) purchased from Vital River Laboratories (Beijing, China) were housed under specific pathogen-free conditions (22 ± 1 °C, $55 \pm 5\%$ humidity, 12-h light/dark cycle) with unrestricted access to autoclaved food and water. Following subcutaneous injection into the right flank using a 27-gauge needle, tumor growth was monitored every 3 days using a digital caliper. Tumor volume (mm³) was calculated as $V = 0.5 \times \text{major axis (D)} \times \text{minor axis}^2 (d)$. When tumors reached 800–1000 mm³ (or 21 days post-injection), mice were euthanized via CO₂ asphyxiation (30% chamber volume displacement rate) followed by cervical dislocation for confirmation. Excised tumors were weighed, photographed, and

divided into two aliquots: fresh-frozen in liquid nitrogen for protein and RNA analysis, and fixed in 4% paraformaldehyde for histology.

2.11 Statistical Analyses

Statistical analyses were performed using SPSS version 22.0 (SPSS, Inc., Chicago, IL, USA). Survival curves were created using the Kaplan-Meier life table method. All quantitative data are expressed as mean \pm standard deviation (SD). An independent sample *t*-test was employed, to compare variables across groups, following a homogeneity of variance test to ensure the validity of the results. The relationships among the identified markers were assessed using Spearman's rank correlation coefficient. A *p*-value of less than 0.05 was considered statistically significant.

3. Results

3.1 The Expression of MAP7 was Increased in Ovarian Cancer

The RNA-seq expression profiles for ovarian cancer were obtained from TCGA, and the normal ovarian tissue datasets were sourced from the GTEx. This dataset contained RNA expression profiles from 424 ovarian cancer tissues and 88 normal tissues. Analysis shows that MAP7 is overexpressed in ovarian cancer ($p < 0.001$) (Fig. 1A). Additionally, the expression level of MAP7 was found to be high across different pathological stages (Fig. 1B). This finding suggests that MAP7 plays an important role in the progression of ovarian cancer. While the MAP7 low-expression group had a slightly better prognosis than the MAP7 high-expression group, this difference was not statistically significant (Fig. 1C). Moreover, immunohistochemical staining from the Human Atlas supported these results (Fig. 1D), and we validated the MAP7 expression patterns using a local ovarian cancer database. Western blot analysis confirmed a notable increase in MAP7 in ovarian cancer tissues compared to adjacent non-cancerous tissues, indicating significant upregulation ($p = 0.0033$) (Fig. 1E). We used the tissue microarray immunohistochemical method to evaluate the expression of MAP7 in 45 cases of ovarian cancer and para-cancerous tissues. Table 1 provides detailed demographic and clinical information for the 45 ovarian cancer patients included in the study. TMA immunohistochemical staining also demonstrated that the expression level of MAP7 in ovarian cancer was much higher than that in para-cancerous tissues ($p < 0.001$) (Fig. 1F, Table 2). Based on the MAP7 staining score analysis, we stratified a cohort of 45 patients into two groups: MAP7-HIGH and MAP7-LOW, to conduct prognostic analysis. The findings revealed a statistically significant association between high MAP7 expression and poorer prognosis in comparison to low MAP7 expression among the patients studied ($p = 0.0129$) (Fig. 1G).

Table 1. Patients' characteristics involved in this research.

Characteristics	No. of patients (N = 45)	%
Age (years)		
≤55	19	42.2
>55	26	57.8
Neoadjuvant chemotherapy		
Yes	21	46.7
No	24	53.3
Pathological stage		
I–II	10	22.2
III–IV	35	77.8
Lymphatic metastasis		
No	21	46.7
Yes	24	53.3
Ascites		
Yes	25	55.6
No	20	44.4

N, number.

Table 2. MAP7 staining H-Score of ovarian cancer tissues is significantly higher than that in para-carcinoma tissue.

	Ovarian cancer	Para-carcinoma tissue	<i>p</i> -value ^a
MAP7	238.6 \pm 41.5	156.8 \pm 27.2	<0.001

^a, Two-sample rank-sum test in SPSS 22.0. MAP7, Microtubule associated protein 7.

3.2 MAP7 Promoted Human Ovarian Cancer Cell Invasion, Migration, and Proliferation

We selected the A2780 and SKOV3 cell lines for *in vitro* experiments. We synthesized small interference RNA and overexpression plasmids to modulate the expression level of MAP7. RT-PCR and Western blot assays confirmed that MAP7 levels were reduced by approximately 30% and elevated by 300% after transfection with siRNA and the expression plasmid, respectively (Fig. 2A–C).

We next used this model to study the effect of MAP7 on the biological function of ovarian cancer cell lines. Compared to the control group, MAP7 knockdown significantly reduced the invasion and migration of ovarian cancer cells. When we overexpressed MAP7, the invasion and migration of ovarian cancer cells were up-regulated (Fig. 2D,E). Similarly, in proliferation experiments, reduced MAP7 expression could inhibit cell proliferation, while overexpression of MAP7 could promote cell proliferation (Fig. 2F,G).

3.3 MAP7 Regulated the Biological Function of Ovarian Cancer Cells by Mediating the Akt/mTOR Signaling Pathway

We examined the expression pattern of the Protein Kinase B/mammalian Target of Rapamycin (Akt/mTOR) signaling pathway in A2780 cells after transfecting with either MAP7 small interfering RNA or an overexpression plasmid (Fig. 3A). The activation or inhibition of the Akt/mTOR

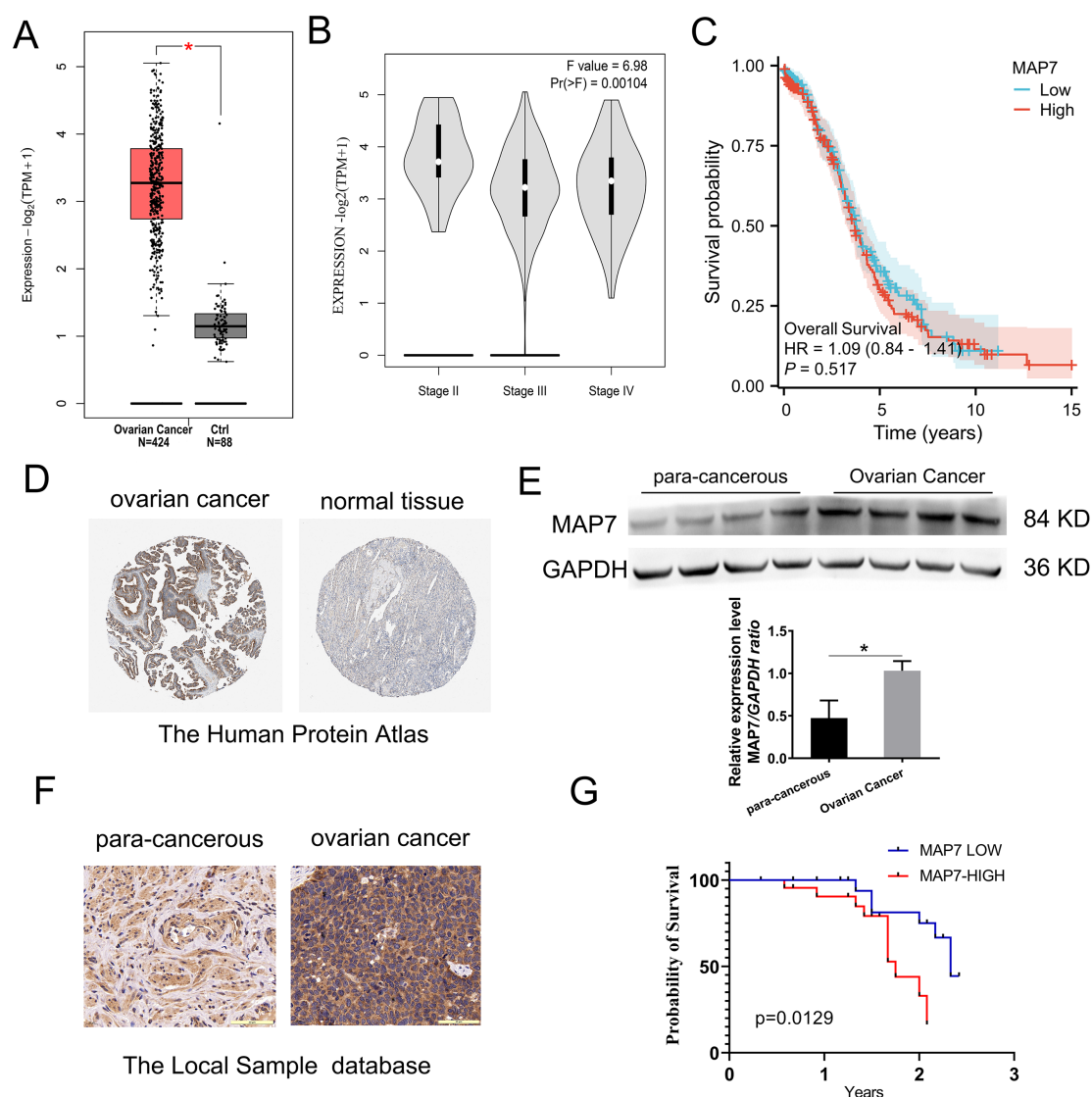


Fig. 1. MAP7 is overexpressed in ovarian cancer. (A–C) The expression profile of MAP7 across all ovarian cancer samples (TCGA database) and paired normal ovarian tissues (GTEx database). (A) MAP7 is upregulated in ovarian cancer ($p < 0.001$). (B) MAP7 expression pattern in different stages of ovarian cancer. (C) MAP7 expression level is not associated with the prognosis of ovarian cancer. (D) TMA analysis indicates that MAP7 levels in ovarian cancer tissues are higher than in normal ovarian tissues, according to The Human Protein Atlas. The magnification of the pictures was 20 \times . (E) Western blot analysis shows that MAP7 is upregulated in ovarian cancer ($p = 0.0033$). (F) TMA analysis shows MAP7 is upregulated in ovarian cancer tissue than para-carcinoma tissue of the local ovarian cancer database. Scale bar = 20 μ m. (G) A prognostic analysis was conducted on 45 patients diagnosed with ovarian cancer ($p = 0.0129$). * $p < 0.05$. TPM, Transcripts Per Kilobase Million; GAPDH, glyceraldehyde-3-phosphate dehydrogenase.

signaling pathway depends on whether MAP7 is increased or decreased (Fig. 3A). This relationship may play a crucial role in enhancing the biological functions of tumor cells. Similarly, we conducted verification using SKOV3 cells. The experimental data confirmed that MAP7 enhances the activation of the Akt/mTOR signaling pathway (Fig. 3B).

3.4 MAP7 Promoted Ovarian Cancer Progression

MAP7 gene knockdown or overexpression in A2780 cells was assessed by using the Lentiviral vector system. A2780 cells were infected with Lentivirus-shScrmble RNA or Lentivirus-the control group of the overexpression experiment (Lentivirus-OV-NC) as a control. Western blot analysis confirmed that MAP7 knockdown efficiency was 80%, while overexpression efficiency was 200% (Fig. 4A).

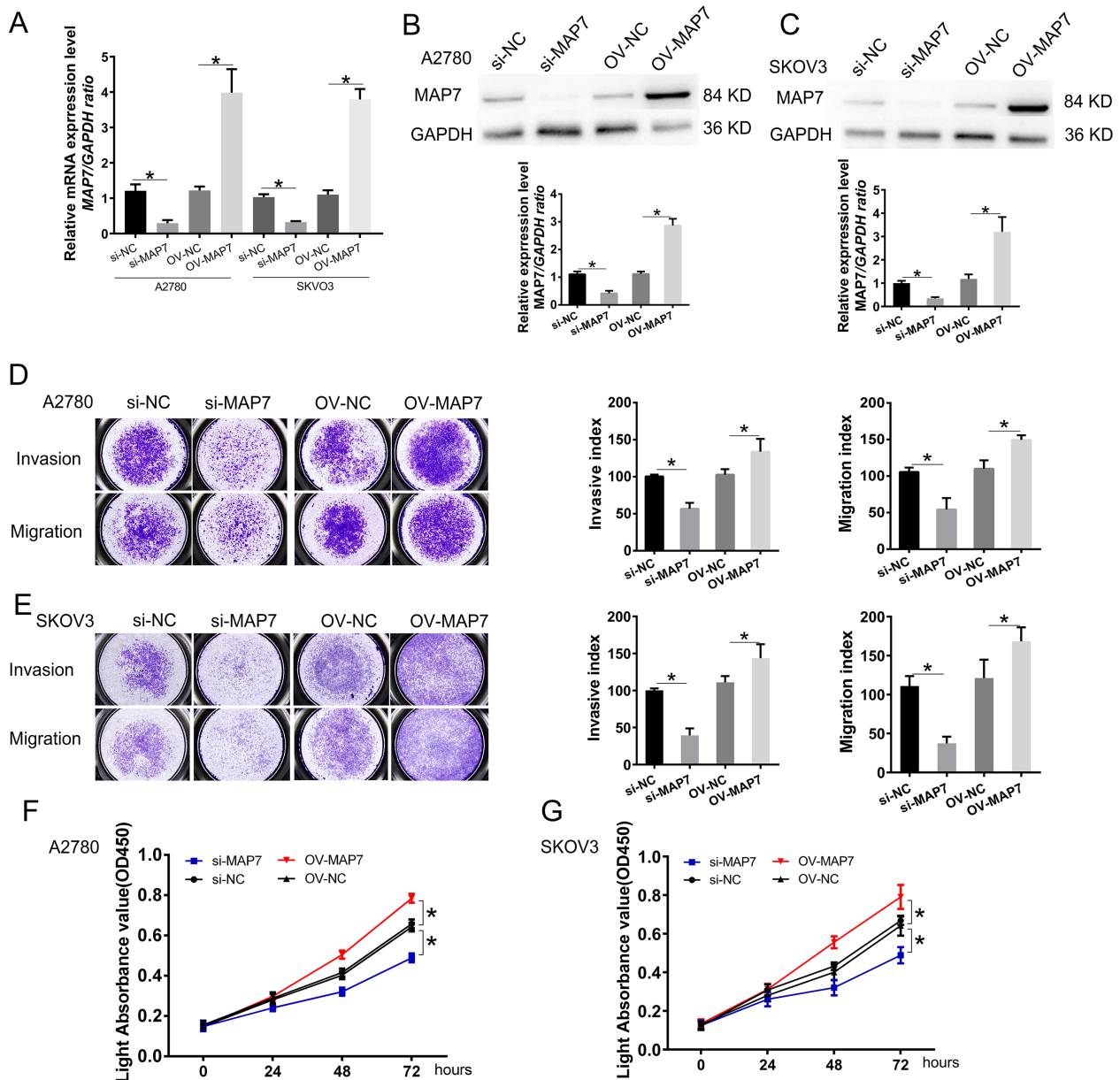


Fig. 2. MAP7 enhances the invasion, migration, and proliferation of human ovarian cancer cells. (A–C) Establishment of ovarian cancer cell model for MAP7 knockdown and overexpression. (A) Real-time PCR to measure the mRNA expression of MAP7 after siRNA or overexpress plasmid transfer (A2780: si-NC vs. si-MAP7 $p = 0.0015$, OV-NC vs. OV-MAP7 $p = 0.0020$; SKOV3: si-NC vs. si-MAP7 $p = 0.0002$, OV-NC vs. OV-MAP7 $p = 0.0001$). (B,C) Western blotting to measure the protein level of the expression of MAP7 after siRNA or overexpress plasmid transfer in A2780 cells (B) (A2780: si-NC vs. si-MAP7 $p = 0.0011$, OV-NC vs. OV-MAP7 $p = 0.0003$) and SKOV3 cells (C) (SKOV3: si-NC vs. si-MAP7 $p = 0.0010$, OV-NC vs. OV-MAP7 $p = 0.0003$). (D,E) Transwell insert assay was carried out to evaluate the role of MAP7 migration and invasion in A2780 cell (D) (invasion: si-NC vs. si-MAP7 $p = 0.0008$, OV-NC vs. OV-MAP7 $p = 0.0479$; migration: si-NC vs. si-MAP7 $p = 0.0061$, OV-NC vs. OV-MAP7 $p = 0.0068$) and SKOV3 cells (E) (invasion: si-NC vs. si-MAP7 $p = 0.0004$, OV-NC vs. OV-MAP7 $p = 0.0426$; migration: si-NC vs. si-MAP7 $p = 0.0012$, OV-NC vs. OV-MAP7 $p = 0.0415$). (F,G) CCK8 assay to measure the cell viability in A2780 cells (F) and SKOV3 cells (G) (A2780: si-NC vs. si-MAP7 $p < 0.0001$, OV-NC vs. OV-MAP7 $p < 0.0001$; SKOV3: si-NC vs. si-MAP7 $p = 0.0005$, OV-NC vs. OV-MAP7 $p = 0.0011$). Each of the tests was replicated three times. Data are presented as mean \pm SD. * $p < 0.05$. PCR, polymerase chain reaction; si-NC, the control group of the knockdown experiment; OV-NC, the control group of the overexpression experiment.

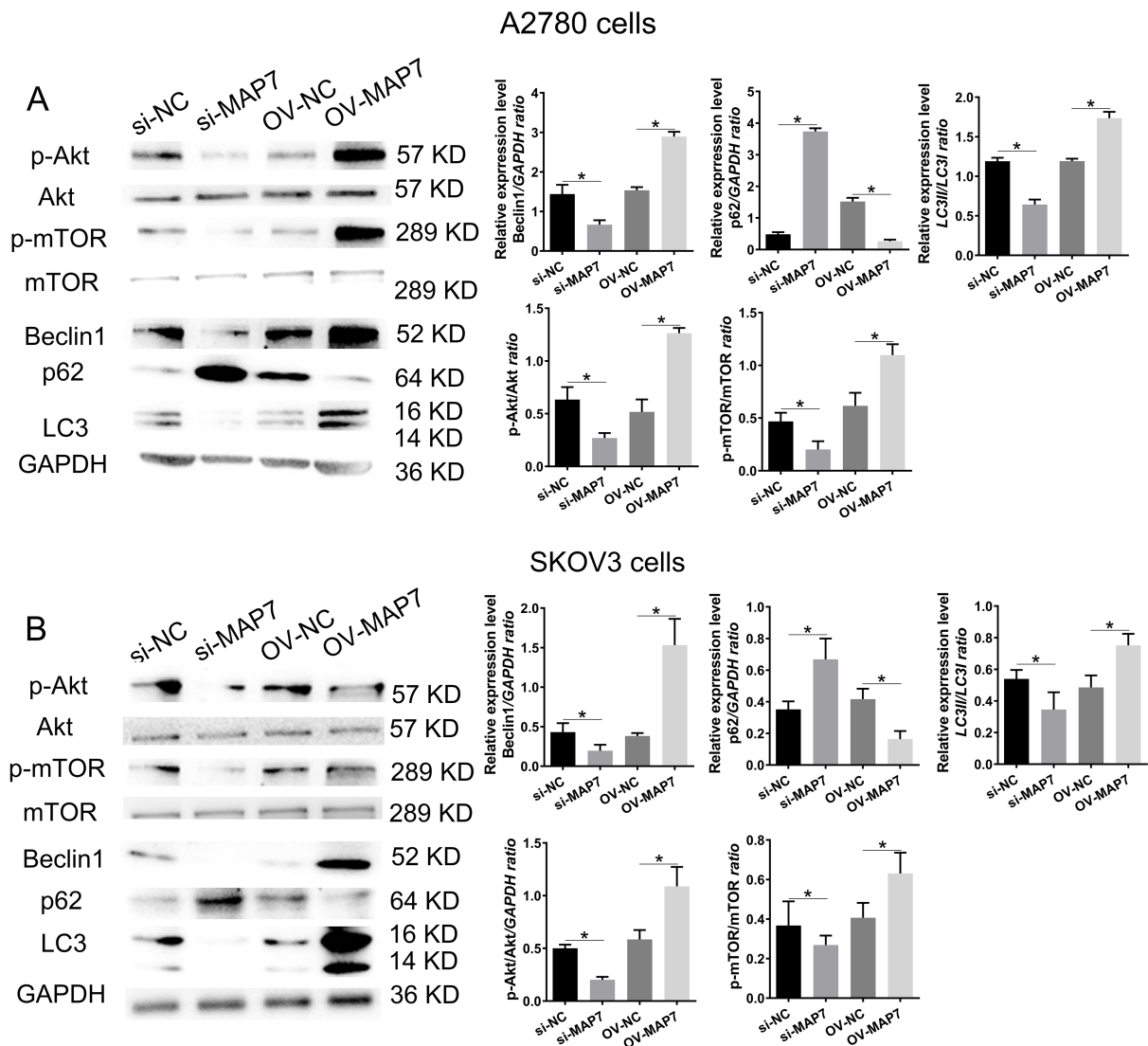


Fig. 3. MAP7 regulates the biological function of ovarian cancer cells by mediating autophagy. Western blotting to measure the expression level of autophagy-related genes after siRNA or overexpress plasmid transfer in A2780 cells (A) (si-NC vs. si-MAP7: Beclin1: $p = 0.068$, p62: $p < 0.001$, LC3B: $p = 0.0021$, p-Akt: $p = 0.0077$, p-mTOR: $p = 0.0159$; OV-NC vs. OV-MAP7: Beclin1: $p < 0.001$, p62: $p < 0.001$, LC3B: $p = 0.0032$, p-Akt: $p = 0.0006$, p-mTOR: $p = 0.0066$) and SKOV3 cells (B) (si-NC vs. si-MAP7: Beclin1: $p = 0.0399$, p62: $p = 0.0177$, LC3B: $p = 0.018$, p-Akt: $p = 0.003$, p-mTOR: $p = 0.026$; OV-NC vs. OV-MAP7: Beclin1: $p = 0.004$, p62: $p = 0.0062$, LC3B: $p = 0.065$, p-Akt: $p = 0.0133$, p-mTOR: $p = 0.0402$). The bar chart shows the statistical results of p-Akt, p-mTOR, Beclin1, p62, and LC3B. Each of the tests was replicated three times. Data are presented as mean \pm SD. * $p < 0.05$. p-Akt, phosphorylated Protein Kinase B; p-mTOR, phosphorylated mTOR; LC3B, Microtubule Associated Protein 1 Light Chain 3 Beta.

To investigate the role of MAP7 in ovarian cancer progression, we injected four groups of six nude mice with either lentivirus MAP7 knockdown cells, overexpression cells, or control cells. The size of the tumor was monitored every 5 days. When the tumor volume in the control group reached 0.5–1 cm³, the experiment was terminated, and tumor tissues were collected. MAP7 knockdown significantly decreased the tumorigenic potential of A2780

cells compared to the control group (Fig. 4B,C). A significant upregulation of MAP7 notably enhanced the tumorigenic potential of ovarian cancer cells (Fig. 4B,C). Then the tumor tissues were identified by HE staining and immunohistochemistry of MAP7 (Fig. 4D). Akt/mTOR signaling pathway is involved in tumor development (Fig. 4E,F). The xenograft experiment in nude mice showed that changes in MAP7 expression significantly affect the tumorigenic po-

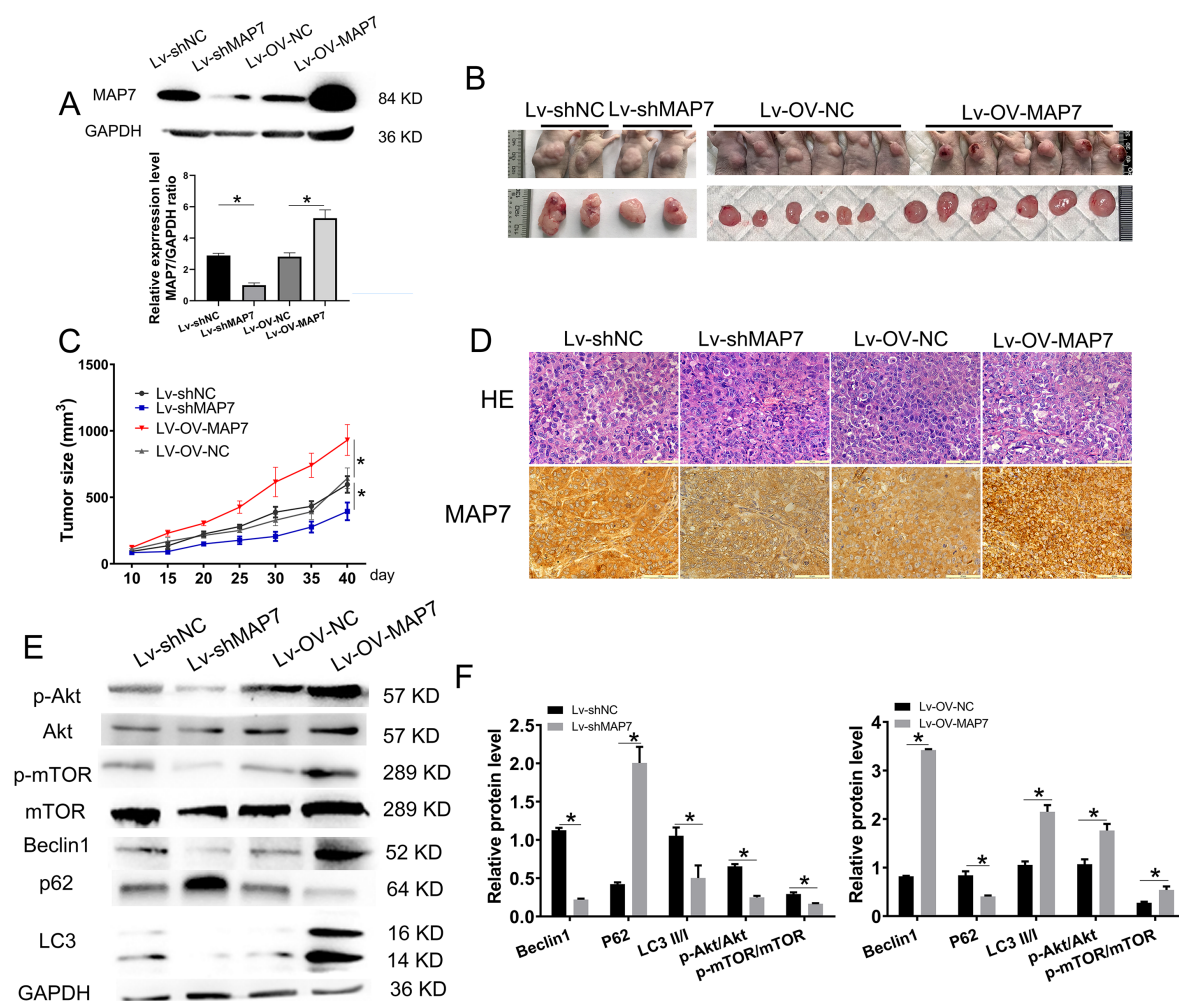


Fig. 4. MAP7 promotes ovarian cancer progression. (A) Construction of A2780 cells with stable MAP7 knockdown or overexpression using a lentivirus system. Western Blot showing the relative expression levels of MAP7 in A2780 cells stably transfected with MAP7 lentivirus (si-NC vs. si-MAP7 $p = 0.0008$, OV-NC vs. OV-MAP7 $p = 0.0138$). (B,C) Tumor formation assays. A2780 cells were injected subcutaneously into the upper back of nude mice (6 mice per group). Mice were examined for tumor formation every 5 days. (D) HE and IHC staining of tumor structure. Scale bar = 20 μ m. (E,F) The bar chart shows the statistical result of p-Akt (si-NC vs. si-MAP7 $p = 0.0035$, OV-NC vs. OV-MAP7 $p = 0.015$), p-mTOR (si-NC vs. si-MAP7 $p = 0.0057$, OV-NC vs. OV-MAP7 $p = 0.024$), Beclin1 (si-NC vs. si-MAP7 $p < 0.001$, OV-NC vs. OV-MAP7 $p = 0.0138$), p62 (si-NC vs. si-MAP7 $p = 0.0017$, OV-NC vs. OV-MAP7 $p = 0.0068$), and LC3B (si-NC vs. si-MAP7 $p = 0.049$, OV-NC vs. OV-MAP7 $p = 0.0022$). Each of the tests was replicated three times. Data are presented as mean \pm SD. * $p < 0.05$. HE, hematoxylin and eosin; GAPDH, glyceraldehyde-3-phosphate dehydrogenase.

tential of ovarian cancer cell lines. This provides further evidence that MAP7 promotes ovarian cancer progression.

4. Discussion

Ovarian cancer (OC) ranks as the second leading cause of cancer-related mortality among women globally, with an annual incidence of approximately 239,000 new cases and 152,000 fatalities [12]. Notably, epithelial ovarian cancer (EOC) represents more than 95% of these ovarian cancers [13,14]. Several risk factors have been identified for EOC, including a family history of the disease, nullipar-

ity, infertility, obesity, endometriosis, advancing age, and genetic predispositions, particularly germline mutations in the breast cancer susceptibility genes *BRCA1* and *BRCA2*. Despite significant progress in diagnostic and therapeutic approaches, the five-year survival rate for patients diagnosed with advanced-stage cancer remains dismally low at 29%, in stark contrast to 92% for those diagnosed at early stages [15]. Only 19% of EOC cases are identified in the early stages of the disease [16], while approximately 75% are identified at an advanced stage [17]. These concerning statistics primarily stem from the absence of effec-

tive early screening methods and the asymptomatic characteristics of EOC, which contribute to delays in diagnosis [17,18]. Consequently, it is crucial to discover novel and effective biomarkers and to investigate more efficient treatment strategies.

In the breast cancer cell line MCF-7, the cervical cancer cell line HeLa, and Ewing's sarcoma cell line TC-7, treatment with Taxol markedly reduced the microtubule-binding activity of MAP7. Concurrently, an increase in MAP7 expression has been linked to augmented resistance to Taxol [19]. Similarly, elevated levels of MAP7 have been documented in cervical cancer patients, showing a positive correlation with poorer prognoses [20–22]. In the lung adenocarcinoma cell line A549, MAP7 has been shown to promote proliferation but appears to have no impact on apoptosis and cell cycle progression [23]. To date, the specific roles and underlying mechanisms of MAP7 in OC remain largely unexplored. Therefore, this study aims to assess the expression levels of MAP7 in OC and to determine its association with patient prognosis.

In this study, the expression of MAP7 was identified to be upregulated in ovarian cancer tissues, based on data from the TCGA-OV dataset. This result was further confirmed by the TMA analysis in local tissue samples and cell lines. To investigate the biological function of MAP7, we measured its mRNA and protein levels in the OC cell line and established both MAP7 knockdown and overexpression models. Our results revealed that silencing MAP7 significantly inhibited viability, migration, invasion, and proliferation in A2780 cells. In contrast, overexpression of MAP7 in the A2780 cells produced the opposite effects. In cervical cancer cell lines, MAP7 has been reported to promote epithelial-mesenchymal transition (EMT) through modulating autophagy [21,24]. The molecular mechanisms of tumor progression are complex, and a single gene can interact with various molecules. In cervical cancer cells, the overexpression of MAP7 promotes cell viability, and motility and suppresses cell apoptosis by activating the MAPK signaling pathway [20]. Furthermore, MAP7 promotes the expression of cyclin D1/cyclin B1, facilitating cell-cycle progression through its interaction with ring finger and CCCH-type domains 1 (RC3H1) in cervical cancer cells [22]. These effects are at least partly mediated by the activation of the canonical IKK/NF- κ B signaling pathway [22].

MAP7 is highly expressed in ovarian cancer tissues, and its expression level significantly correlates with late-stage disease, high-grade tumors, and poor clinical outcomes. Functional experiments have shown that inhibiting MAP7 markedly impairs the proliferative, migratory, and invasive capabilities of ovarian cancer cells while promoting apoptosis. This effect is closely linked with the modulation of EMT and the Wnt/ β -catenin signaling pathway by MAP7 [24].

Additionally, MAP7 may influence its biological functions within cancer cells through various alternative

mechanisms. Fu *et al.* (2016) [25] conducted a comprehensive analysis of microRNA profiles and identified a significant correlation between MAP7 expression and 145 microRNAs. In patients with cytogenetically normal acute myeloid leukemia who exhibit high MAP7 expression, oncogenic microRNAs such as miR-196b and miR-99a are up-regulated, while tumor-suppressive microRNAs like miR-193a and miR-27a are down-regulated [25]. Notably, miR-16, which targets MAP7, has been shown to modulate cell proliferation without affecting apoptosis or the progression of the cell cycle in cancerous cells [23]. Additionally, circular RNA circNF1 enhances gastric cancer cell proliferation by targeting the miR-16/(MAP7 and AKT3) axis. Additionally, plasma exosomal circRNA NIMA-related kinase 9 (CircNEK9) promotes the proliferation, migration, and invasion capabilities of gastric cancer cells by interacting with the miR-409-3p/MAP7 axis [26]. Collectively, these findings suggest that MAP7 serves as a molecular target for non-coding RNAs and plays a significant role in regulating cancer cell motility and tumor advancement [27–29].

MAP7 offers a unique opportunity in ovarian cancer management. It serves both as a target for disrupting aggressive phenotypes and as a biomarker for improving patient stratification. To effectively translate these concepts into clinical practice, it is essential to prioritize the development of inhibitors, validate biomarkers, and encourage interdisciplinary collaboration. However, we must also systematically address significant challenges, including tool development, ensuring model accuracy, and managing clinical trial logistics.

5. Conclusions

Research indicates that MAP7 is upregulated in ovarian cancer patients and plays a crucial role in regulating the biological functions of ovarian cancer cells by mediating the Akt/mTOR signaling pathway. Future studies are necessary to achieve a comprehensive understanding of the molecular mechanism by which MAP7 contributes to ovarian cancer progression. Given its association with Akt/mTOR signaling and tumorigenicity in preclinical models, MAP7 is a promising candidate for further investigation as a potential therapeutic target.

Availability of Data and Materials

The datasets used and analyzed during the current study are available from the corresponding author on reasonable request.

Author Contributions

GC, XR designed the research study. GC and ZQ performed the research. XS analyzed the data. GC drafted the manuscript. All authors contributed to critical revision of the manuscript for important intellectual content. All au-

thors read and approved the final manuscript. All authors have participated sufficiently in the work and agreed to be accountable for all aspects of the work.

Ethics Approval and Consent to Participate

Patients' tissues in our study were approved by the ethics committee of Beijing chaoyang hospital, affiliated to the Capital Medical University (approval number: 2020-S-66). Collection and use of human ovarian cancer tissue and para-cancerous tissue samples and informed consent was obtained from all the subjects. All procedures performed in animal studies were approved by the Animal Research Ethics Committee of Capital Medical University (AEEI-2022-006). The methods were carried out in accordance with the approved guidelines and the Declaration of Helsinki.

Acknowledgment

Not applicable.

Funding

This research received no external funding.

Conflict of Interest

The authors declare no conflict of interest.

References

- [1] Dion L, Lavoué V. Ovarian Cancer: Latest Advances and Prospects. *Journal of Clinical Medicine*. 2021; 10: 5919. <https://doi.org/10.3390/jcm10245919>.
- [2] McMullen M, Karakasis K, Rottapel R, Oza AM. Advances in ovarian cancer, from biology to treatment. *Nature Cancer*. 2021; 2: 6–8. <https://doi.org/10.1038/s43018-020-00166-5>.
- [3] Garrido MP, Fredes AN, Lobos-González L, Valenzuela-Valderrama M, Vera DB, Romero C. Current Treatments and New Possible Complementary Therapies for Epithelial Ovarian Cancer. *Biomedicines*. 2021; 10: 77. <https://doi.org/10.3390/biomedicines10010077>.
- [4] Ranade H, Paliwal P, Chaudhary AA, Piplani S, Rudayni HA, Al-Zharani M, *et al.* Predicting Diagnostic Potential of Cathepsin in Epithelial Ovarian Cancer: A Design Validated by Computational, Biophysical and Electrochemical Data. *Biomolecules*. 2021; 12: 53. <https://doi.org/10.3390/biom12010053>.
- [5] Mirza MR. Highlights in ovarian cancer from the 2021 American Society of Clinical Oncology Annual Meeting: commentary. *Clinical Advances in Hematology & Oncology: H&O*. 2021; 19 Suppl 19: 20–23.
- [6] Bhat KMR, Setaluri V. Microtubule-associated proteins as targets in cancer chemotherapy. *Clinical Cancer Research: an Official Journal of the American Association for Cancer Research*. 2007; 13: 2849–2854. <https://doi.org/10.1158/1078-0432.CCR-06-3040>.
- [7] Cassimeris L, Spittle C. Regulation of microtubule-associated proteins. *International Review of Cytology*. 2001; 210: 163–226. [https://doi.org/10.1016/s0074-7696\(01\)10006-9](https://doi.org/10.1016/s0074-7696(01)10006-9).
- [8] Sood R, Bader PI, Speer MC, Edwards YH, Eddings EM, Blair RT, *et al.* Cloning and characterization of an inversion breakpoint at 6q23.3 suggests a role for Map7 in sacral dysgenesis. *Cytogenetic and Genome Research*. 2004; 106: 61–67. <https://doi.org/10.1159/000078563>.
- [9] Gallaud E, Caous R, Pascal A, Bazile F, Gagné JP, Huet S, *et al.* Ensconsin/Map7 promotes microtubule growth and centrosome separation in *Drosophila* neural stem cells. *The Journal of Cell Biology*. 2014; 204: 1111–1121. <https://doi.org/10.1083/jcb.201311094>.
- [10] Chaudhary AR, Lu H, Krementsova EB, Bookwalter CS, Trybus KM, Hendricks AG. MAP7 regulates organelle transport by recruiting kinesin-1 to microtubules. *The Journal of Biological Chemistry*. 2019; 294: 10160–10171. <https://doi.org/10.1074/jbc.CRA119.008052>.
- [11] Hooikaas PJ, Martin M, Mühlethaler T, Kuijntjes GJ, Peeters CAE, Katrukha EA, *et al.* MAP7 family proteins regulate kinesin-1 recruitment and activation. *The Journal of Cell Biology*. 2019; 218: 1298–1318. <https://doi.org/10.1083/jcb.201808065>.
- [12] Bray F, Ferlay J, Soerjomataram I, Siegel RL, Torre LA, Jemal A. Global cancer statistics 2018: GLOBOCAN estimates of incidence and mortality worldwide for 36 cancers in 185 countries. *CA: A Cancer Journal for Clinicians*. 2018; 68: 394–424. <https://doi.org/10.3322/caac.21492>.
- [13] Torre LA, Trabert B, DeSantis CE, Miller KD, Samimi G, Runowicz CD, *et al.* Ovarian cancer statistics, 2018. *CA: A Cancer Journal for Clinicians*. 2018; 68: 284–296. <https://doi.org/10.3322/caac.21456>.
- [14] Prat J. Ovarian carcinomas: five distinct diseases with different origins, genetic alterations, and clinicopathological features. *Virchows Archiv: an International Journal of Pathology*. 2012; 460: 237–249. <https://doi.org/10.1007/s00428-012-1203-5>.
- [15] Reid BM, Permuth JB, Sellers TA. Epidemiology of ovarian cancer: a review. *Cancer Biology & Medicine*. 2017; 14: 9–32. <https://doi.org/10.20892/j.issn.2095-3941.2016.0084>.
- [16] Iorio MV, Visone R, Di Leva G, Donati V, Petrocca F, Casalini P, *et al.* MicroRNA signatures in human ovarian cancer. *Cancer Research*. 2007; 67: 8699–8707. <https://doi.org/10.1158/0008-5472.CAN-07-1936>.
- [17] Lheureux S, Gourley C, Vergote I, Oza AM. Epithelial ovarian cancer. *Lancet (London, England)*. 2019; 393: 1240–1253. [https://doi.org/10.1016/S0140-6736\(18\)32552-2](https://doi.org/10.1016/S0140-6736(18)32552-2).
- [18] Lheureux S, Braunstein M, Oza AM. Epithelial ovarian cancer: Evolution of management in the era of precision medicine. *CA: a Cancer Journal for Clinicians*. 2019; 69: 280–304. <https://doi.org/10.3322/caac.21559>.
- [19] Gruber D, Faire K, Bulinski JC. Abundant expression of the microtubule-associated protein, ensconsin (E-MAP-115), alters the cellular response to Taxol. *Cell Motility and the Cytoskeleton*. 2001; 49: 115–129. <https://doi.org/10.1002/cm.1026>.
- [20] Tang N, Lyu D, Chang JF, Liu ZT, Zhang Y, Liu HP. Enhanced expression of microtubule-associated protein 7 functioned as a contributor to cervical cancer cell migration and is predictive of adverse prognosis. *Cancer Cell International*. 2020; 20: 354. <https://doi.org/10.1186/s12935-020-01446-x>.
- [21] Zhang L, Liu X, Song L, Zhai H, Chang C. MAP7 promotes migration and invasion and progression of human cervical cancer through modulating the autophagy. *Cancer Cell International*. 2020; 20: 17. <https://doi.org/10.1186/s12935-020-1095-4>.
- [22] Zhang R, Li L, Chen L, Suo Y, Fan J, Zhang S, *et al.* MAP7 interacts with RC3H1 and cooperatively regulate cell-cycle progression of cervical cancer cells via activating the NF- κ B signaling. *Biochemical and Biophysical Research Communications*. 2020; 527: 56–63. <https://doi.org/10.1016/j.bbrc.2020.04.008>.
- [23] Yan X, Liang H, Deng T, Zhu K, Zhang S, Wang N, *et al.* The identification of novel targets of miR-16 and characterization of their biological functions in cancer cells. *Molecular Cancer*. 2013; 12: 92. <https://doi.org/10.1186/1476-4598-12-92>.
- [24] Chen Q, Li S, Fu F, Huang Q, Zhang R. MAP7 drives EMT and cisplatin resistance in ovarian cancer via wnt/ β -catenin signal-

- ing. *Heliyon*. 2024; 10: e30409. <https://doi.org/10.1016/j.heliyon.2024.e30409>.
- [25] Fu L, Fu H, Zhou L, Xu K, Pang Y, Hu K, *et al*. High expression of MAP7 predicts adverse prognosis in young patients with cytogenetically normal acute myeloid leukemia. *Scientific Reports*. 2016; 6: 34546. <https://doi.org/10.1038/srep34546>.
- [26] Yu L, Xie J, Liu X, Yu Y, Wang S. Plasma Exosomal Circ-NEK9 Accelerates the Progression of Gastric Cancer via miR-409-3p/MAP7 Axis. *Digestive Diseases and Sciences*. 2021; 66: 4274–4289. <https://doi.org/10.1007/s10620-020-06816-z>.
- [27] Shen Y, Ori-McKenney KM. Microtubule-associated protein MAP7 promotes tubulin posttranslational modifications and cargo transport to enable osmotic adaptation. *Developmental Cell*. 2024; 59: 1553–1570.e7. <https://doi.org/10.1016/j.devcel.2024.03.022>.
- [28] Wang X, Cao X, Wu Y, Chen T. MAP7 promotes proliferation and migration of breast cancer cells and reduces the sensitivity of breast cancer cells to paclitaxel. *Journal of Chemotherapy (Florence, Italy)*. 2023; 35: 231–239. <https://doi.org/10.1080/1120009X.2022.2082349>.
- [29] Wang R, Xie S, He Y, Zheng R, Zhang M, Jin J, *et al*. MAP7 Promotes Breast Cancer Cell Migration and Invasion by Regulating the NF- κ B Pathway. *Annals of Clinical and Laboratory Science*. 2022; 52: 721–730.